An overview of soil erosion modelling compatible with RUSLE approach

Massimo Fagnano · Nazzareno Diodato · Ines Alberico · Nunzio Fiorentino

Abstract Different approaches were used to model soil losses in the Sele River basin (southern Italy) characterized by data scarcity. The suitability of models interpolating different sources of data was evaluated with the aim to suggest similar methodologies in other regions where data availability is not sufficient to use the more complex and detailed models. The first approach is based on the concept of the balance between driving and resisting forces. Rainfall is considered as both a driving and resisting factor: the rain erosivity not only increases with its amount and intensity but also enhances the protective effect of vegetation. The long-term erosion rate of the basin resulted mainly affected by local land-cover conditions that showed a more dramatic effect than the variability of rain erosivity. In the period during which soils were protected by natural woodlands, net erosion rates were extremely low, while the elimination of forest (AD 1780–1810) increased erosion that reached annual rates from 20 to 300 Mg km^{-2}. The second approach is a revised and scale-adapted Foster–Meyer–Onstad model suitable for scarce input data (CliFEM = Climate Forcing and Erosion Modelling). This new idea was addressed to develop a monthly Net Erosion model (NER) and gross erosion was estimated from the sediment delivery ratio (SDR). From this approach it is clear that the erosion regime was clearly autumnal with a mean rate of 8 Mg ha^{-1} per month. The long-term average soil erosion highlighted, since 1990, a more irregular temporal pattern, with the highest annual erosion (200 Mg ha^{-1}) in 2002. The third approach combines the revised universal soil loss equation (RUSLE) with GIS–geospatial technology. Regression Ordinary Kriging (ROK)-based maps of erosive rainfall were made on annual and monthly basis. The months following soil tillage (from August to November) have become even more hazardous for soil erosion, with values higher than 80% of total yearly soil losses, because in this period the highest rainfall erosivity is coupled to the lowest soil cover due to soil tillage at the end of summer. In these conditions soil can be protected only by the agro-environmental measures aimed at reducing soil erodibility and at increasing soil cover, such as conservative soil tillage (i.e. sod seeding) and perennial cover crops in orchards and vineyards.

Keywords Soil erosion · Modelling · GIS · RUSLE

M. Fagnano (✉) · N. Fiorentino
Dipartimento Ingegneria Agraria e Agronomia del Territorio,
Università degli Studi "Federico II" di Napoli,
Via Università 100, 80055 Portici, Italy
e-mail: fagnano@unina.it

N. Diodato
Met European Research Observatory, GEWEX-CEOP Network,
World Climate Research Programme, 82100 Benevento, Italy

I. Alberico
Centro Interdipartimentale di Ricerca Ambiente,
Università degli Studi "Federico II" di Napoli,
Via Mezzocannone 16, 80134 Naples, Italy

1 Introduction

An accurate estimation of rainfall aggressiveness plays a major role in land management and protection. The spatial

70

Rend. Fis. Acc. Lincei (2012) 23:69–80

variability of rain erosivity is often considered as a major source of uncertainty in the soil loss models (Boardman 1993; Wang et al. 2002). Although several studies have focused on the spatial pattern of climate aggressiveness with different methodologies, only a few have recently studied how it is affected by both climate and its annual extremes. This was mainly due to the scarcity of erosivity–data in individual months or years, especially in mountainous and developing countries, where hourly and sub-hourly pluviometrical data are not available.

Land use change has been recognized throughout the Earth as one of the most important factors influencing the occurrence of rainfall-driven geomorphological processes. This is particularly true in Mediterranean conditions where the low organic matter content of soils (Jones and Montanarella 2004; Zhang and Nearing 2005) causes high erodibility values: in the Sele River basin the RUSLE erodibility K-factor was estimated 0.026 ± 0.0049 Mg h MJ^{-1} mm^{-1} on the average (Diodato et al. 2011a). This work evaluated the possibility to estimate soil erodibility by interpolating both data obtained from direct measurements and data estimated with auxiliary terrain data and land system class memberships. Although human judgment involved in this information is an additional source of uncertainty, combining more types of data using a geostatistical approach can be a successful strategy for improving soil erodibility mapping in undersampled regions. The proposed approach offers effective spatial predictions, and it is exportable to regions where financial costs for soil sampling are not feasible (Diodato et al. 2011a).

When rainstorms happen over tilled soil or unvegetated lands, soil mobilization and sediment yield can exacerbate the erosion processes, implying an impact over both agricultural lands, with nutrient and soil loss, and coastal areas, with remodelling of the natural beach (Kosmas et al. 1997). This particularly occurs in areas as the Mediterranean Europe, where weather variability and very intense land use may increase erosion processes (Diodato et al. 2011b).

With the purpose to skip over these drawbacks, several methodologies were applied in different areas of southern Italy. In this paper, the different models used in Campania region (Sele and Calore basins) are presented and their results are discussed and compared.

2 Historical-empirical approach

The concept of the balance between driving and resisting forces in sediment budget modelling was originally proposed by Douglas (1967) that provided an empirical climate index converted into metric units:

$$E_{\mathrm{P}} = \frac{1.631 \cdot (0.03937 \cdot P_{\mathrm{e}})^{2.3}}{1 + 0.007 \cdot (0.03937 \cdot P_{\mathrm{e}})^{3.3}} \tag{1}$$

where E_{P} is the suspended sediment yield (m^3 km^{-2} year^{-1}); P_{e} is the effective precipitation (mm), that is precipitation minus potential evapotranspiration; where the numerator represents the driving force of rainfall and the denominator the vegetation-protection factor. This model is suitable for large basins and is not universally applicable.

Later on, Thornes (1990) built a finer model to simulate monthly erosion by water runoff that can be expressed as:

$$E_{\mathrm{T}} = \sum_{j=1}^{12} \left(k \cdot Q^a \cdot S^d \cdot e^{-iV} \right) \tag{2}$$

where E_{T} is the annual erosion amount (mm year^{-1}) over the months from 1 (January) to December (12); k is soil erodibility; Q is the runoff (mm month^{-1}); a is the flow power coefficient (1.66); S is the tangent of slope (m m^{-1}); d is the empirical slope constant (2.0 from Mulligan and Wainwright 2004); V is the vegetation cover (%); and i is the erosion exponential function (0.07 from Mulligan and Wainwright 2004).

The application of a parsimonious scale-adapted erosion model (ADT) from the original Thornes (1990) and Douglas (1967) algorithms, allowed to reconstruct annual net erosion (ANE) upon multisecular timescales (Diodato 2006).

Soil erosion by water mainly occurs when the detachment of particles and their subsequent transportation are subjected to a greater driving force than the protective effect of vegetation, that is related to the reduction of the kinetic energy of rainfall, the increase of soil surface roughness, aggregate stability and infiltration. Within this process the rainfall is considered as both a driving and resisting factor. The erosive influence of rainfall increases with its amount and intensity, but, the protective effect of vegetation also increases with precipitation amount. The balance between these forces can be expressed, according the following revised Douglas-and-Thornes-non-linear equation, as:

$$ANE_{\mathrm{ADT}j} = k \cdot \frac{R_j^m \cdot e^{-b\mathrm{VC}j}}{(\mathrm{Med_w} \cdot (P))^c} \tag{3}$$

where ANE_{ADT} is the net soil loss from basin in the jth year, in Mg km^{-2} year^{-1}; R is the rainfall erosivity factor (MJ mm ha^{-1} h^{-1} year^{-1}); $e^{(-b \cdot \mathrm{VC})}$ is the Thornes's vegetation erosion exponential function that represents the short-term resisting force, where VC is the vegetation cover (%), and b is a parameter in function of the ratio of rill to interrill erosion with bare soil conditions (Thornes 1990); the term at denominator is the pattern of long-term resisting force occurring on a window timescales, represented by ground cover erosive-resistance climatic function

(after Douglas 1967), where precipitation median value $\text{Med}_w(P)$ is expected on a time moving window (w) antecedent the year j, with $w = 7$ years.

The four empirical coefficients ($k = 0.0168$; $m = 2$; $b = -0.050$ and $c = 0.70$) and the length of the window (w) were estimated by minimizing the sum squared errors (SSE) over η data:

$$\text{SSE} = \sum_{j=1}^{\eta} \left(\text{ANE}_{\text{measured}(\eta)} - \text{ANE}_{\text{ADT}(\eta)} \right)^2 \quad (4)$$

So, a goodness-of-fit measure that minimizes the absolute errors rather than relative errors for high soil loss values is used to develop a model that estimates net erosion for use (Toy et al. 2002).

In preinstrumental period R was evaluated following Diodato and Ceccarelli (2005):

$$R = 0.88 \left[0.0897(6 + \text{WIS}_s)(2 + \sigma_{\text{WI}}^2)P - 1{,}306 \right] + 1{,}271 \quad (5)$$

where WIS_S is the weather index sum which was obtained by summing monthly WI values in June–October period following the classification: rainy without floods (WI $= +1$), stormy or rainy with floods (WI $= +2$), droughts (WI $= 0$); the variance of the WI index (σ_{WI}^2) over January–December period was taken into account as an indicator of the erosivity (after Aronica and Ferro 1997); P is the annual precipitation amount (mm).

This approach was applied in the Calore River basin (3,015 km^2 in southern Italy; Fig. 1), where input-data generation and interpretation of the results were also supported by documented hydrogeomorphological events that occurred before and after land deforestation (Diodato 2006).
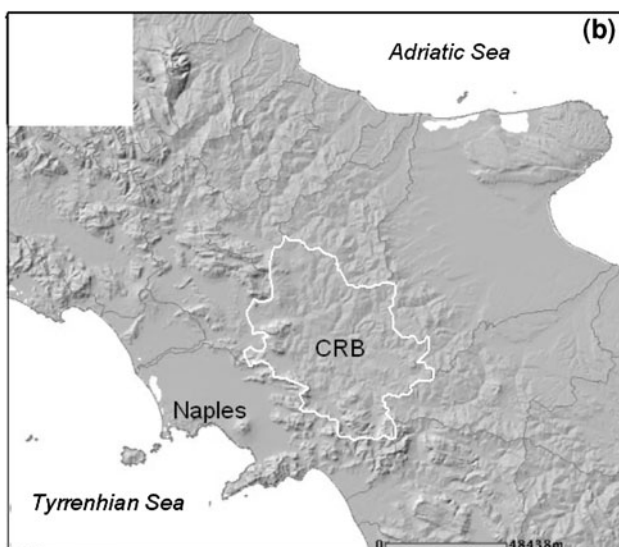

Fig. 1 Geographic location of the Calore River Basin (CRB)

The rain erosivity (histogram in Fig. 2) showed a clear smoothed period after several years of high climatic variability during the first two centuries of the series. In particular, 18th and 19th centuries had very frequent and extreme storms. Vegetation patterns change (the 3 images in Fig. 2) shows a soft land use until the beginning of 19th century, with vast areas of territory covered by woods. In this period, net erosion rates were extremely low (about 10 Mg km^{-2}). The abolition of feudality in 1806 and the start of an agrarian reform aimed at the distribution of the feudal and municipal lands to poor citizens in the whole of southern Italy (Rovito 2001) led to the cultivation of mountain areas and to the elimination of woods. At the beginning of this period (AD 1780–1810), erosion increased and reached annual rates of about 20–100 Mg km^{-2}. In the following period (1811–1860), long-term curve fitting (white curve in Fig. 2) indicated that soil erosion exponentially increased to exceed the threshold of 300 Mg km^{-2}.

The results from Diodato (2006) suggested that the land use has a more dramatic increase on erosion rates than to the variability of rain erosivity.

3 CliFEm approach

Diodato et al. (2009) proposed a revised and scale-adapted Foster–Meyer–Onstad model (Foster et al. 1977) with the acronym CliFEM (Climate Forcing and Erosion Modelling). This new idea was addressed to develop a monthly time scale invariant Net Erosion model (NER), with the aim to consider the different erosion processes operating at different time scales during 1973–2007 period in the Sele River Basin located in southern Italy from southern Campania to Western Basilicata regions (Fig. 3). The sediment delivery ratio approach (SDR) was applied to obtain an indirect estimate of the gross erosion too.

CliFEM approach was developed to include the major conceptual advantages of some erosion models. However, while NER model was largely determined by the required experimental data, the SDR model was constrained by weakness of the available data in Sele River Basin. Another important characteristic of the NER model was to consider the different erosion processes at different time scales (from monthly to annual). The major weakness of this approach may be in the sediment data quality, and in the consequent uncertainty in sediment delivery ratio, that is a critical point in many models (Borselli 2006).

In this study, a sub-routine introduced by Foster et al. (1977) was expanded and adapted to take into account the runoff shear stress effect on soil detachment for single storms. The new time scale-invariant process-based Net Erosion (NERTSI) model was used for predicting monthly

72

Rend. Fis. Acc. Lincei (2012) 23:69–80

Fig. 2 Reconstructed (ANE$_{ADT}$)—Annual Net Erosion during 1675–2004 period (*lower row*) with rain erosivity exceeding 1,000 MJ mm ha^{-1} h^{-1} year^{-1} (*higher row*), and vegetation cover (*middle row*). Rearranged from Diodato ([2006](#))
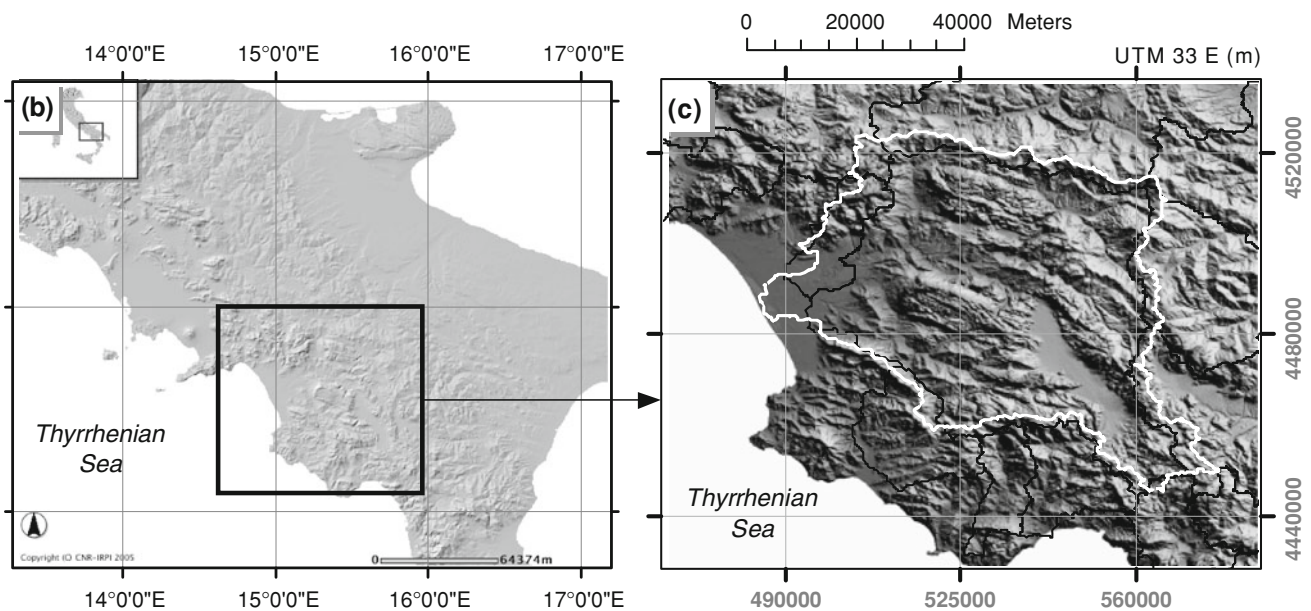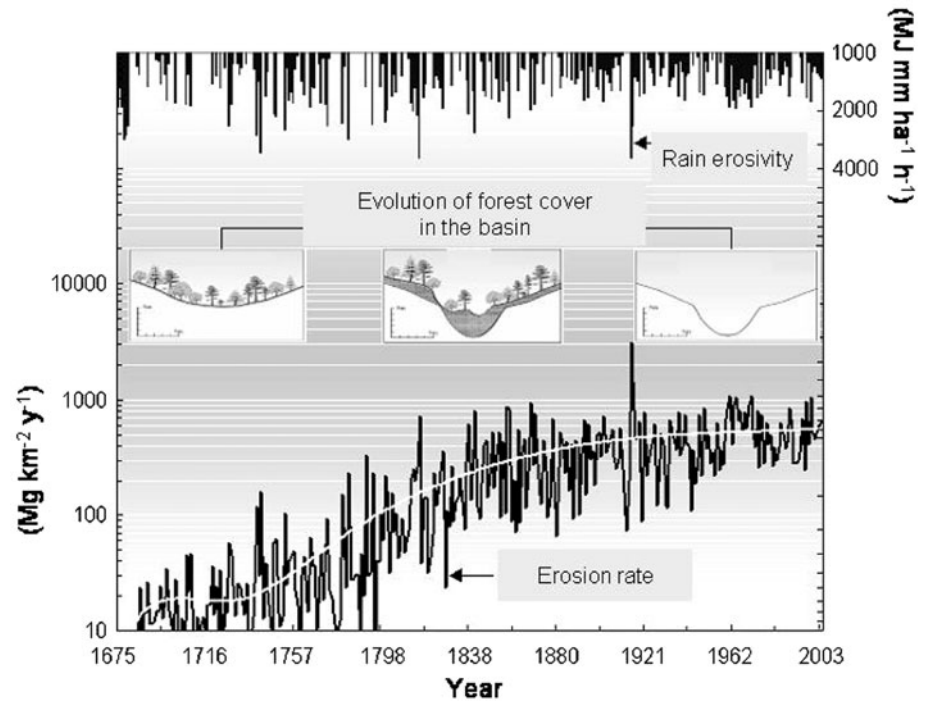

Fig. 3 Morphology of the Sele River Basin from GlobalMapper

net erosion over medium basins (around 3,000 km^2). The hydrological ecosystem module, considers the interrelationships of rainfall erosivity, runoff, erodibility and vegetation cover:

$$\mathrm{NER_{TSI}} = K \cdot (\alpha \cdot \overline{\mathrm{EI}}_m + \beta \cdot \overline{Q}_m)^{\psi} \\ \cdot \exp\left[(-\gamma \cdot (\overline{\mathrm{NDVI}}_m \cdot 100)\right] \quad (6)$$

where the first term in bracket is the modified erosivity factor as adapted by Foster et al. ([1977](#)), while the second

term is the modified vegetation erosion exponential function, as adapted by Thornes ([1990](#)); K is the RUSLE erodibility factor (Mg h MJ^{-1} mm^{-1}) changing with basin soils, that was set equal to 0.0362 (an approximate range of K values can be founded in van der Knijff et al. [2000](#)); α, β and ψ are empirical parameters equal to 0.40, 0.60 and 2.05, respectively; γ is the parameter of the vegetation exponential function, set equal to 0.04, earlier placed equal to 0.07 by Thornes ([1990](#)).

Monthly rainfall erosivity at gauged station EI_m (MJ mm ha^{-1} h^{-1} $month^{-1}$) was derived from rainfall measurements in the Italian area, according to RUSLE scheme (Diodato 2005):

$$EI_m = 0.1174 \cdot (\sqrt{p} \cdot d^{0.53} \cdot h^{1.18}) \tag{7}$$

where p is the monthly precipitation amount (mm), d is the monthly maximum daily rainfall (mm), and h is the monthly maximum hourly rainfall (mm). In this approach, d and h are descriptors of the extreme rainfalls (storms and heavy showers, respectively) (Diodato 2005).

With lack of experimental measurements (after 1994 year in this specific case), monthly runoff (Q_m) was estimated by adapting the Vandewiele et al. (1992) approach:

$$\overline{Q}_m = \eta_m \left[\overline{p}_m - \overline{AET}_m \left(0.5 - \exp\left(-\frac{\overline{p}_m}{\overline{AET}_m} \right) \right) \right] \tag{8}$$

where p_m and AET_m are the average values of rainfalls and actual evapotranspiration, respectively; η_m are the monthly experimental coefficients related to soil.

The simulation of daily SDR made with the Soil and Water Assessment Tool—SWAT (Arnold and Williams 1995) was conceptually revised and adapted to the monthly scale by the equation:

$$SDR_m = \left(a + b \frac{\overline{Q}_m}{\overline{EI}_m} \right)^c \tag{9}$$

where the terms of the ratio are those above described; a, b and c are three coefficients equal to 0.035, 0.010 and 0.50, respectively, derived imposing a values of SDR-long-term equal to 0.19, which, in turn, was supported by expert knowledge (Borselli, personal communication), and checked by CSIRO abaco (Lu et al. 2003) on the basis of the basin area and the storm duration. The well-known relationship to convert net erosion to gross soil loss is:

$$GER = \frac{NER}{SDR} \tag{10}$$

where GER is the monthly gross soil loss, NER is the net erosion, and SDR is the sediment delivery ratio.

Since the effects of soil erosion on soil productivity depend on the thickness of these soils, it is possible to define the tolerable amount of soil loss when the soil thickness of an area is known. The tolerable soil loss (TSL) may be calculated using the Bhattacharyya et al. (2007) approach:

$$TSL = \frac{PLD \cdot D \cdot S_d}{T} \tag{11}$$

where PLD is the proportion of land downgraded to at least the next depth class (%, assumed equal to 15%), T is the time (years, assumed equal to 100), D is the bulk density of the soil (assumed equal to 1.4 Mg m^{-3}), S_d is the soil depth (assumed equal to 130 cm).

Using this approach, erosion regime resulted clearly autumnal with values around a mean rate of 8 Mg ha^{-1} per month. The frequency distribution was strongly skewed and bimodal for net erosion (Fig. 4a1), as well as for gross erosion (figure not shown). If annual gross erosion amounts were ordered from the highest to the lowest value over the 35-year period, the resulting curve was an exponential equation:

$$y = a \cdot \exp(b \cdot t) \tag{12}$$

where y is soil loss, t is the year number, and a and b are constants (Fig. 4b1).

Figure 4 shows that in only 10 of the 35 years the soil losses exceeded the long-term average (horizontal dotted line), with soil erosion accounting for 60% of the total estimated soil eroded. These examples illustrate the dominance of relatively few events in the determination of long-term erosion average.

The long-term average soil erosion was very high (73 Mg ha^{-1} per year $\pm$ 58 Mg ha^{-1}). Progressive yearly averaged values during 1973–2007 period showed a changeable trend with short intervals characterized by negligible soil losses, followed by periods with erosion above the tolerable soil loss, and often above severe erosion rates too. At the beginning of the 1990s, it was evident a more irregular temporal pattern, with the highest annual erosion (200 Mg ha^{-1}) in 2002.

4 RUSLE approach

This study combines the revised universal soil loss equation (RUSLE) with GIS–geospatial technology, to explore erosion-prone areas in the Sele River agricultural basin (Campania–Basilicata regions, southern Italy).

The average soil loss (E) due to water erosion per unit area and per year was quantified using RUSLE (Renard et al. 1997):

$$E = R \cdot K \cdot LS_{2D} \cdot C \cdot P \tag{13}$$

where E is the annual soil loss (Mg ha^{-1}) averaged upon a period selected according to erosivity factor (R), 30 years (1957–1986) in this work; R is the rainfall erosivity factor [MJ mm $(ha\ h)^{-1}$]; K is the soil erodibility factor [Mg ha h $(ha\ MJ\ mm)^{-1}$]; LS_{2D} is the two-dimensional topographic factor, with L the length and S slope; C is the cover and management factor; and P is the conservation support-practices factor. LS, C and P are dimensionless values.

4.1 Rain erosivity

Changes in the climate time patterns may have important effects on the interaction among erosive rainfalls,
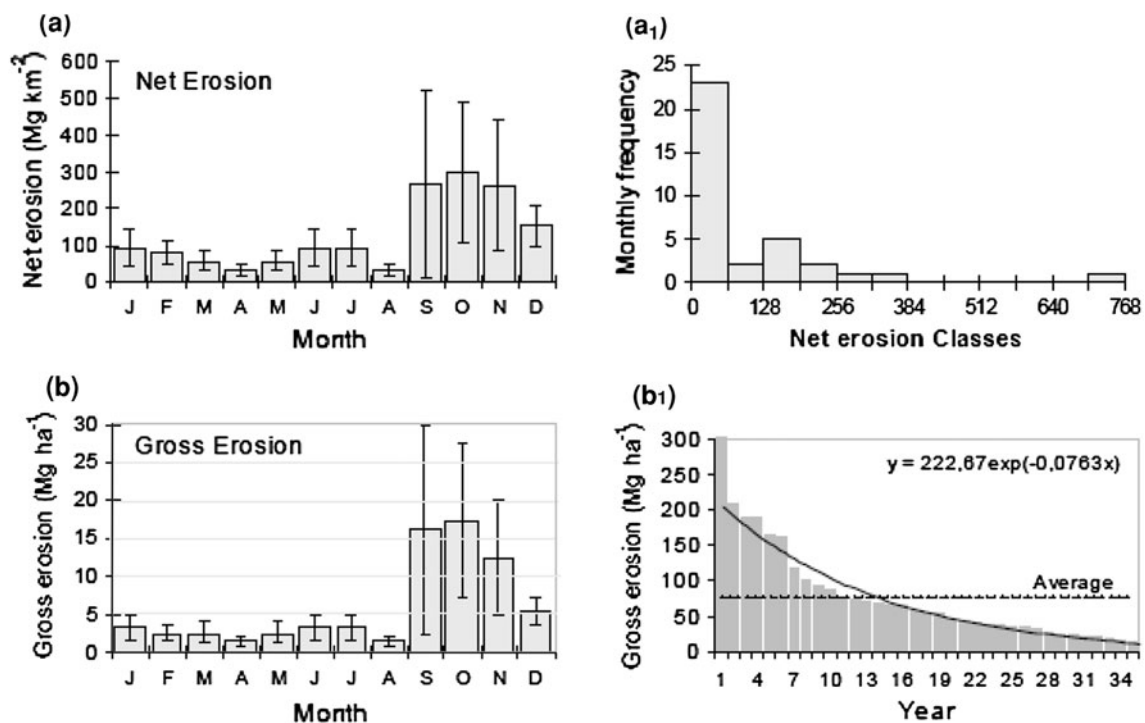
Fig. 4 Long-term monthly predicted average for net erosion (**a**), and gross erosion (**b**) with related 95% confidence interval; net erosion frequency distribution (**a1**), and ordered gross erosion amount (histogram in **b1**) for the 35-year period (1973–2007) with overimposed the related average value (*horizontal dotted line*) and exponential model (*curve*) at Sele River Basin

vegetation covers and runoff. In Mediterranean areas, erosion is particularly pronounced both in the semiarid regions (200–300 mm year^{-1}), and in the sub-humid ones (900–1,500 mm year^{-1}) and the strong variability in annual precipitation with frequent events of extreme rainfalls may result in increasing susceptibility of regional erosion (Boardman and Favis-Mortlock 2001).

During the last few decades, many extreme events were recorded and several researches detected increasing trends in these extreme hydrometeorological phenomena: for north-eastern Italy, with a reduction of the return period (Brunetti et al. 2001), for Portugal (de Santos Loureiro and de Azevedo Coutinho 1995) and for southern Italy Apennines (Diodato 2004a) with an increase in rainfall erosivity.

The concept of rainfall erosivity was introduced and developed in the context of the Universal Soil Loss Equation (USLE; Wischmeier and Smith 1958), and reviewed in Revised USLE (RUSLE; Renard et al. 1997). The erosive empirical index (EI_{30}) is a numerical descriptor (Wischmeier and Smith 1958) and the long-term average annual erosivity R-factor (MJ mm ha^{-1} h^{-1}year^{-1}) is the sum of the EI_{30} values occurring during a mean year.

Generally, long series of meteorological variables do not include sub-hourly rainfall intensities and this limits the possibility of applying the USLE/RUSLE for estimating historical series of erosivity values. To deal with it, Diodato (2004b) developed a parsimonious annual erosivity-based

model on easily available rain-predictors deriving from individual years, as well as, from long-term averaged predictors. In this last form, Diodato's model, can be rewritten as:

$$R = 12.142 \cdot (0.01 \cdot \text{Pr} \cdot d \cdot h)^{0.6446} \qquad (14)$$

where Pr is the average annual rainfall (mm), d is the annual maximum daily rainfall (mm), and h is the annual 1 h maximum rainfall (mm).

In the Sele River Basin (SRB), Diodato et al. (2011b) proposed a GIS-based approach for improvement mapping of R-factors, and of the consequent soil losses hazard. Regression Ordinary Kriging (ROK) was applied in this study.

A parsimonious framework was firstly developed for designing spatial variability of long-term average rain erosivity and its extremes annuality within assigned return period (T). This methodology was successively applied for a test site located in a mountainous agricultural basin of the Campania Region (southern Italy). In the third step, the approach was set to extend the information with stochastic geospatial tools in GIS, using mainly daily records of 62 rain-stations of the Department of Civil Protection established by Campania and Basilicata Regional Monitoring Networks.

From our results (Diodato et al. 2008; Diodato and Fagnano 2011), annual rain erosivity ranges from 600 to
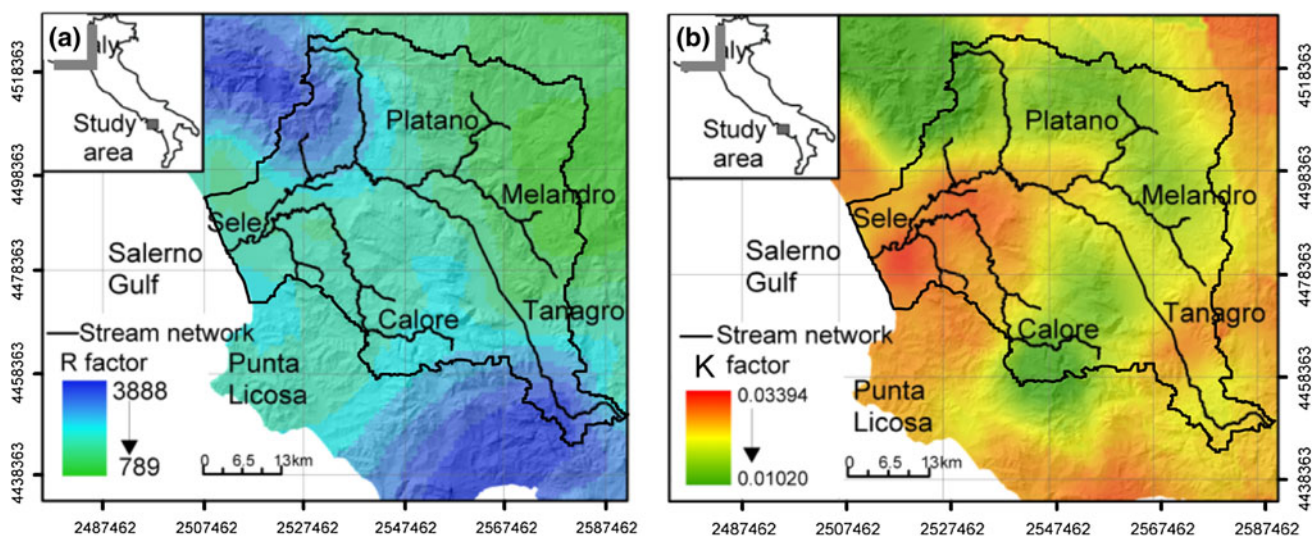
Fig. 5 Regression kriged map for long-term average rain erosivity (**a**) and soil erodibility (**b**) (from: Diodato and Fagnano 2011 and Diodato et al. 2011a, respectively)

4,000 MJ mm ha^{-1} h^{-1}, with mean and standard deviation of 2,000 ± 883 MJ mm ha^{-1} h^{-1} (Fig. 5a).

In Central Mediterranean area, autumn is a season prone to these extremes. Precipitation anomalies for the month of September of many years of decade 1998–2007 (data not shown) were unusually positive until 100 mm month^{-1}.

4.2 Soil erodibility

Evaluation of soil erodibility is an important task for Mediterranean lands, in which fertility and crop yield are significantly affected by soil erosion. The soil physico-chemical parameters affecting soil erodibility are highly variable in space and sample measurements are generally not enough for assessing its spatial variability with an acceptable level of uncertainty at scales of practical interest.

Diodato et al. (2011a) proposed a new procedure for estimating the pattern of soil erodibility across the Sele Basin (southern Italy), where soil properties have been measured on a limited number of sparse samples. The proposed procedure is similar to the one proposed by Abbaspour et al. (1998). Soil erodibility data calculated by directly measured soil properties in a limited number of sample locations are integrated with soil erodibility data estimated from site-specific regression equations. These regression equations (Local Topotransfer Functions, LTFs) provide estimates of soil erodibility from other auxiliary variables, such as terrain attributes and specific information regarding land system class memberships, which show significant correlation with soil erodibility sampled data. The combination of estimated and sampled data generates a larger composed data set usable as input for composed

data ordinary kriging (CO_OK) interpolation method. This procedure can be used as an alternative to other types of multivariate geostatistical techniques in areas characterized by a limited number of sampled data, but where it is possible to obtain estimated data from other auxiliary variables. LTFs can be calibrated with primary and auxiliary data pairs available at same locations and they can be then applied to estimate values of the primary data at locations for which auxiliary data, but not primary data are available.

The RUSLE K-factor (Mg h MJ^{-1} mm^{-1}) has been computed according to the equation suggested by Torri et al. (1997):

$$K = 0.0293(0.65 - \mathrm{Dg} + 0.24\mathrm{Dg}^2)e^{\{-0.021\frac{OM}{C}-0.00037(\frac{OM}{C})^2-4.02C+1.72C^2\}} \quad (15)$$

where C is the fraction of total clay (expressed as a fraction), OM the percentage of organic matter, and Dg is the base 10 logarithm of the geometric mean of diameter size distribution.

When the number of sampled data is not sufficient for reliable spatial estimates of the primary variable, auxiliary variables such as terrain attributes and soil class membership can be used as potential predictors to estimate the primary variable in supplementary locations using Local Topotransfer Functions (Salski 2006; Wessolek et al. 2008). A prerequisite for the development of these functions is the availability of auxiliary variables in the same locations, covering representative value ranges in which these variables are expected to vary within the study area (Illian et al. 2008). Similar to the pedotransfer functions (Matula and Spongrovà 2007), LTFs can be linear or non-linear regression equations. In this case study, we

explored the possibility to use two types of auxiliary variables:

- class memberships according to the land system classification of Campania Region edited by Di Gennaro (2002) following an integrated approach suggested by FAO (1995) and Dalal-Clayton and Dent (2001);
- terrain attributes, such as elevation, terrain slope and aspect.

Elevation has been selected among other terrain attributes, being most suitable for inferring soil erodibility K-factor, based on a Pearson correlation test. The LTFs have been then applied to 109 new locations. Sampled (114 samples) and estimated (109) soil erodibility values resulted in a composed data set of 223 samples. The soil erodibility map derived from this new approach (Diodato et al. 2011a) used for improving the spatial variability estimates is reported in Fig. 5b. The estimates of the areal average over the whole region and the standard deviation is 0.026 ± 0.0049 Mg h MJ^{-1} mm^{-1}, with a median of 0.028 Mg h MJ^{-1} mm^{-1}. The range of K values was from 0.010 to 0.045 Mg h MJ^{-1} mm^{-1}, thus within the range estimated by the European Soil Bureau at a larger scale (Van der Knijff et al. 2000). Spatially related alterations in soil erodibility were found, with increasing values from limestone mountain areas (Platano, Melandro and Calore sub-basins) to the Sele alluvial plain, where a very high erodibility core was evident (>0.03 Mg h MJ^{-1} mm^{-1}).

4.3 Slope and length factors

The slope (S) and length (L) factors represent the topography of the landscape and define the effects of slope angle and slope length on the sheet and rill erosion. The LS factor was computed using the upslope contributing area per width unit of contour instead of individual slope length and slope angle to capture the effect of flow convergence (Desmet and Govers 1996; Mitasova et al. 1996, 1998). The LS factor was assessed in a continuous form, using the following equation (Mitasova et al. 1996):

$$\mathrm{LS} = (m + 1)(A/a_0)^m [\sin(b/b_0)]^n \qquad (16)$$

where A is the upslope contributing area, b is the slope angle, a_0 and b_0 are the standard USLE length (22.1 m) and slope (0.09), respectively, m and n are parameters. The Digital Elevation Model (DEM) of the study area, with a 50×50 m grid cell resolution, was applied to Eq. 16 in a continuous form.

In detail, using the hydrological extension of ESRI–ArcGIS, release 9.1, four main steps were followed with the aim to define the upslope contributing area: (a) the sinks in the DEM were identified and filled to obtain the depressionless DEM (Hutchinson 1989); (b) the depressionless DEM was used as input to determine the flow direction; (c) the flow direction was used as input to determine the flow accumulation; (d) a threshold value of 125 cells, based on the comparison of flow accumulation and stream network of the Campania Region Technical Cartography at scale 1:5.000 (Regione Campania 1998), was applied to the flow accumulation grid to identify the area where runoff is active. The slope angle was calculated in degree using the slope algorithm of Spatial Analyst and successively changed in radiant. The parameter m, according to Wischmeier and Smith (1978), was defined using a grid with variable exponent 0.2, 0.3, 0.4 and 0.5 for slope gradient <1, 1–3, 3–4.5 and >5%, respectively. The parameter n was defined as 1.3 (Moore et al. 1993).
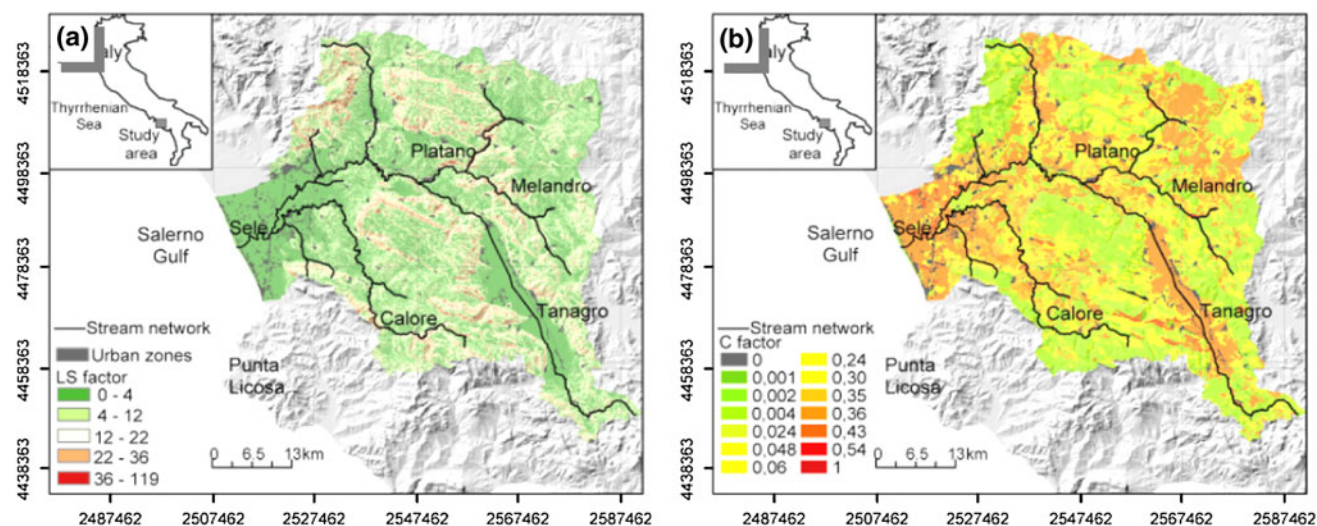

Fig. 6 Map of slope and length RUSLE-factors (**a**) and vegetation cover (**b**)

The LS spatial distribution map for the SRB (Diodato et al. 2011b), is reported in Fig. 6a.

4.4 Vegetation cover and land management factors

The C-factor value describes the effect of vegetation cover on erosion (Table 1). It is the ratio between soil loss of study area and the corresponding loss from continuous tilled bare fallow. Based on the Corine Land Use map of Campania Region at scale 1:50.000, 27 land use classes were identified with specific C-factor values (Table 1 from Angeli 2004; Bakker et al. 2008; Märker et al. 2008). We assigned a C-factor value of 0 for a a priori assumption to urban areas and other land uses (Bakker et al. 2008) where soil is covered or not present (i.e. bare rocks, water courses). We assigned slightly increasing values (from 0.001 to 0.003) to conifer, mixed and broad-leaved forests since in the study area the broad-leaved forests are mainly represented by chestnut trees that are deciduous and therefore reduce winter protection of soil in comparison with conifers (Angeli 2004). Pastures were assimilated to alfalfa

established stand (0.02), while natural grassland was assimilated to unmanaged grassland (0.05). Moors and heathland and sclerophyllous vegetation were assimilated to shrublands. However, because we did not have data to distinguish dense from sparse shrubs, we used their average C-factor value (0.05). Complex cultivation patterns and agro-forestry areas were assimilated to arable dense tree cover, while annual crops associated with permanent crops were assimilated to arable medium tree cover (0.20 and 0.25, respectively). For fruit trees and berry plantations, olive groves and vineyards, the C-factor values 0.30, 0.30 and 0.45 were used (Angeli 2004; Märker et al. 2008), because they were adopted in Tuscany Region that has similar conditions with respect to southern Italy. Considering that arable land in SRB is a mixture (both in space and in time) of different crops, in some cases also both irrigated and not irrigated, a long-term average value was used (0.30 from Bakker et al. 2008). Land mainly occupied by agriculture, with significant areas of natural vegetation was assimilated to arable sparse tree cover (0.30), while it was assigned a higher value (0.36 from Angeli 2004) to the

Table 1 C-factor values of the different Corine land covers

CLC code	Land use	Value	Source
111	Continuous urban fabric	0	Märker et al. (2008)
112	Discontinuous urban fabric	0	Märker et al. (2008)
121	Industrial or commercial units	0	Märker et al. (2008)
122	Road and rail networks and associated land	0	Bakker et al. (2008)
141	Green areas inside urban fabric	0	Bakker et al. (2008)
332	Bare rocks	0	Bakker et al. (2008)
511	Water courses	0	Märker et al. (2008)
312	Coniferous forest	0.001	Angeli (2004)
313	Mixed forest	0.002	Angeli (2004)
311	Broad-leaved forest	0.003	Angeli (2004)
231	Pastures	0.020	Bakker et al. (2008)
324	Transitional woodland shrub	0.040	Märker et al. (2008)
321	Natural grassland	0.050	Bakker et al. (2008)
322	Moors and heathland	0.050	Bakker et al. (2008)
323	Sclerophyllous vegetation	0.050	Bakker et al. (2008)
242	Complex cultivation patterns	0.200	Bakker et al. (2008)
244	Agro-forestry areas	0.200	Bakker et al. (2008)
241	Annual crops associated with permanent crops	0.250	Bakker et al. (2008)
222	Fruit trees and berry plantations	0.300	Angeli (2004)
223	Olive groves	0.300	Märker et al. (2008)
211	Non-irrigated arable land	0.300	Bakker et al. (2008)
212	Irrigated arable land	0.300	Bakker et al. (2008)
243	Agriculture land, with significant areas of natural vegetation	0.300	Bakker et al. (2008)
333	Sparsely vegetated areas	0.360	Angeli (2004)
221	Vineyards	0.450	Märker et al. (2008)
131	Mineral extraction sites	1.000	Bakker et al. (2008)
331	Beaches, dunes, sands	1.000	Bakker et al. (2008)

sparsely vegetated areas. We assigned the maximum value (1.00) to mineral extraction sites, beaches, dunes and sands, because these lands are not protected by vegetation.

From this map (Fig. 6b), it is clear that the vegetation cover with the lowest protection of soil is mainly concentrated in the internal and in the coastal flat areas towards the mouth of the Sele River (arable land). Other large internal hilly areas characterized by olive groves and vineyard are also evident. The basin area is covered by forest (55%), agricultural area (43%) and urbanized areas (2%). In detail, broad-leaved forest (68%) and natural grassland (16%) prevail in the forest area. Complex cultivation patterns (15%) and fruit tress, vineyard and olive groves (16%) prevail in the agricultural areas.
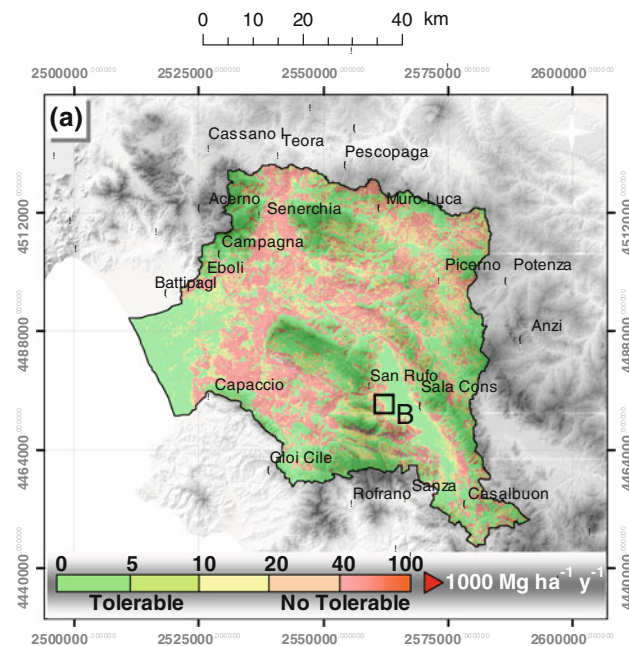

Fig. 7 Long-term average of RUSLE-based soil loss rate

4.5 Soil losses estimation

The RUSLE-based soil loss rate was reported in the Fig. 7. The values ranged from 20 to 150 Mg ha^{-1} year^{-1} with mean rates of 53 ± 43 Mg ha^{-1} year^{-1}. Using the *soil delivery ratio* (SDR), as defined in Diodato et al. (2009), about the 80% of the eroded soils were trapped in the depressions and valleys during the transport process via drainage network.

Considering a tolerance threshold of 20 Mg ha^{-1} year^{-1} for soil depth >100 cm, soil loss can be classified as tolerable and no tolerable (Fig. 7). The 32% of the SRB was subjected to no-tolerable soil losses, and about 7% was affected by catastrophic erosion (e.g., rates >80 Mg ha^{-1} year^{-1}).

Considering that the months following soil tillage (from August to November) are the most hazardous for soil erosion in SRB (Figs. 4, 8), with values higher than 80% of total yearly soil losses (Diodato et al. 2009), all the agro-environmental measures aimed at reducing soil erodibility and at increasing soil cover during this period (such as conservative soil tillage, perennial cover crops in orchards and vineyards, mulching and sod seeding) have to be strengthened and spread. The adoption of such agro-environmental measures, will be increasingly important in a perspective of climate change considering that just in September a strong increase of erosion has been calculated in the last 10 years in comparison with the previous period (Fig. 8), as already pointed out by several authors (Nearing et al. 2004; Zhang and Nearing 2005; González-Hidalgo et al. 2007).

The effectiveness of conservative cropping systems was also confirmed by field experiments made nearby SRB, in which soil cover with wheat crop residues allowed an almost complete reduction of erosion in comparison with tilled soil (2.291 Mg ha^{-1} year^{-1}), showing soil losses (0.015 Mg ha^{-1} year^{-1}) not different from the permanent meadow (0.004 Mg ha^{-1} year^{-1}) as a consequence of an
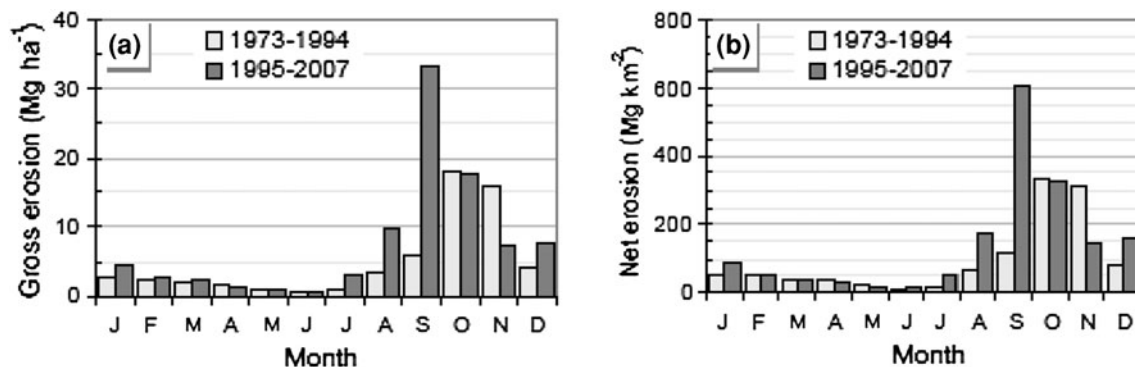

Fig. 8 Comparison of the monthly average for predicted gross erosion (**a**), and net erosion (**b**) between the 1973–1994 and 1995–2007 periods (from Diodato et al. 2009)

intense rain event (maximum intensity = 32.4 mm h^{-1}) recorded on 2 August 1995 (Fagnano et al. 2000).

5 Conclusions

The different approaches used for estimating soil losses in the Sele basin of Campania region gave similar results (73 and 53 Mg ha^{-1} year^{-1} on the average) and highlighted some features of soil erosion in Mediterranean areas:

1. The erosion rate of the basin resulted mainly affected by local land-cover conditions that showed a more dramatic effect than the variability of rain erosivity.
2. Particularly vulnerable are hilly and valley areas, where high rainfall erosivity is coupled with reduction of the vegetation cover at the beginning of autumn.
3. Arable lands, orchards and vineyards are the most vulnerable land uses. The months following soil tillage (from August to November) are the most hazardous for soil erosion, with values higher than 80% of total yearly soil losses because in this period the highest rainfall erosivity is coupled with the lowest soil cover due to soil tillage at the end of summer.
4. In these conditions soil can be protected only by the strengthening and spreading of the agro-environmental measures aimed at reducing soil erodibility and at increasing soil cover, such as conservative soil tillage (i.e. sod seeding) and perennial cover crops in orchards and vineyards, which will be increasingly important in the perspective of climate change.

References

Abbaspour KC, Schulin R, van Genuchten MT, Schlappi E (1998) An alternative to cokriging for situations with small sample sizes. Math Geol 30:259–274

Angeli L (2004) Valutazione del rischio erosione applicazioni del modello RUSLE, Centro Ricerche Erosione Suolo, Report 2004, 21 p. http://www.lamma-cres.rete.toscana.it/rapporti/2004/2.pdf. Accessed 23 Sept 2009

Arnold JG, Williams JR (1995) A continuous time water and sediment routing model for large basins. J Hydraul Div–ASCE 121:171–183

Aronica G, Ferro V (1997) Rainfall erosivity over the Calabrian region. J Hydrol Sci 42:35–48

Bakker MM, Govers G, Van Doorn A, Quetier F, Chouvardas D, Rounsevell M (2008) The response of soil erosion and sediment export to land-use change in four areas of Europe: the importance of landscape pattern. Geomorphology 98:213–226

Bhattacharyya T, Babu R, Sarkar D, Mandal C, Dhyani BL, Nagar AP (2007) Soil loss and crop productivity model in humid subtropical India. Curr Sci India 93:1397–1403

Boardman J (1993) The sensitivity of downland arable land to erosion by water. In: Thomas DSG, Allison RJ (eds) Landscape sensitivity. John Wiley & Sons, Chichester, pp 211–228

Boardman JD, Favis-Mortlock T (2001) How will future climate change and land-use change affect rates of erosion on agricultural land. In: Soil erosion research for the 21st Century. Am Soc Agric Biol Eng, Honolulu, Hawaii, pp 498–501, 3–5 Jan 2001

Borselli L (2006) Valutazione dell'erodibilità del suolo in applicazioni a scala di bacino. In: Costantini EAC (ed) Metodi di valutazione dei suoli e delle terre. Cantagalli, Siena, pp 197–222

Brunetti M, Maugeri M, Nanni T (2001) Changes in total precipitation, rainy days and extreme events in northeastern Italy. Int J Climatol 21:861–871

Dalal-Clayton B, Dent D (2001) Knowledge of the land. Land resources information and its use in rural development. Oxford University Press, New York

de Santos Loureiro N, de Azevedo Coutinho M (1995) Rainfall changes and rainfall erosivity increase in the Algarve (Portugal). Catena 24:55–67

Desmet PJJ, Govers G (1996) Comparison of routing algorithms for digital elevation models and their implications for predicting ephemeral gullies. J Geograph Inform Syst 10:311–331

Di Gennaro A (2002) I sistemi di terre della Campania. Carta 1:250.000 e Legenda. Selca, Firenze

Diodato N (2004a) Local models for rainstorm-induced hazard analysis on Mediterranean river-torrential geomorphological systems. Nat Hazard Hydrol Earth Syst Sci 4:389–397

Diodato N (2004b) Estimate RUSLE's rainfall factor in the part of Italy with a Mediterranean rainfall regime. Hydrol Earth Syst Sci 8:103–107

Diodato N (2005) Geostatistical uncertainty modelling for the environmental hazard assessment during single erosive rainstorm events. Environ Monit Assess 105:25–42

Diodato N (2006) Modelling net erosion responses to enviroclimatic changes recorded upon multisecular timescales. Geomorphology 80:164–177

Diodato N, Ceccarelli M (2005) Erosive rainfall reconstruction since 1580 AD in Calore River Basin (Southern Italy). SCODA Report, University of Sannio. Available on line at: http://www.scoda.unisannio.it/Papers/Archive/Diodato_R_reconstruction%20in%20CRB.pdf

Diodato N, Fagnano M (2011) A simple geospatial model climate–based for designing erosive rainfall pattern. In: Nemr AE (ed) The environmental pollution and its relation to climate change. Nova Science Publishers, New York (in Press)

Diodato N, Ceccarelli M, Bellocchi G (2008) Decadal and century-long changes in the reconstruction of erosive rainfall anomalies at a Mediterranean fluvial basin. Earth Surf Proc Land 33:2078–2093

Diodato N, Fagnano M, Alberico I (2009) CliFERM—Climate forcing and erosion response modelling at long-term Sele River Research Basin (Southern Italy). Nat Hazard Earth Syst Sci 9:1693–1702

Diodato N, Fagnano M, Alberico I, Chirico GB (2011a) Mapping soil erodibility from composed dataset in Sele River Basin, Italy. Nat Hazards 58:445–457

Diodato N, Fagnano M, Alberico I (2011b) Geospatial–and–visual modeling for exploring sediment source areas across the Sele river landscape Italy. Italian J Agronomy 6:85–92

Douglas I (1967) Man, vegetation and sediment yield of rivers. Nature 215:925–928

80

Rend. Fis. Acc. Lincei (2012) 23:69–80

Fagnano M, Mori M, Carone F, Postiglione L (2000) Sistemi colturali per l'Appennino meridionale: Nota II. Deflussi ed erosione, Rivista di Agronomia 34:55–64 (in Italian)

Foster GR, Meyer LD, Onstad CA (1977) A runoff erosivity factor and variable slope length exponents for soil loss estimates. T ASAE 20:683–687

González-Hidalgo JC, Peña-Monné JL, de Luis M (2007) A review of daily soil erosion in Western Mediterranean areas. Catena 71: 193–199

Hutchinson MF (1989) A new procedure for gridding elevation and stream line data with automatic removal of spurious pits. J Hydrol 106:211–232

Illian J, Penttinen A, Stoyan H, Stoyan D (2008) Statistical analysis and modelling of spatial point patterns. John Wiley and Sons Ltd, Chichester

Jones RJA, Montanarella L (2004) Organic matter in the soils of southern Europe. European Soil Bureau Technical Report, Luxembourg

Kosmas C, Danalatos N, Cammeraat LH, Chabart M, Diamanopoulos J, Farand R, Gutierrez L, Jacob A, Marques H, Martinez-Fernandez J, Mizara A, Moustakas N, Nicolau JM, Oliveros C, Pinna G, Puddu R, Puigdefabregas J, Roxo M, Simao A, Stamou G, Tomasi N, Usai D, Vacca A (1997) The effect of land use on runoff and soil erosion rates under Mediterranean conditions. Catena 29:45–59

Lu H, Moran CJ, Prosser IP, Raupach RM, Olley J, Petheram C (2003) Sheet an rill erosion sediment delivery to streams: a basin wide estimation at hillslope to Medium catchment scale, Report E to Project D10012, CSIRO Technical Report 15/03

Märker M, Angeli L, Bottai L, Costantini R, Ferrari R, Innocenti L, Siciliano G (2008) Assessment of land degradation susceptibility by scenario analysis: a case study in Southern Tuscany, Italy. Geomorphology 93:120–126

Matula S, Spongrovà K (2007) Pedotransfer function application for estimation of soil hydrophysical properties using parametric methods. Plant Soil Environ 53:149–157

Mitasova H, Hofierka J, Zlocha M, Iverson LR (1996) Modeling topographic potential for erosion and deposition using GIS. Int J Geograph Inform Sci 10:629–641

Mitasova H, Mitas L, Brown WM, Johnson D (1998) Multidimensional soil erosion/deposition modeling and visualization using GIS. University of Illinois, Urbana-Champaign, Final report for USA CERL

Moore ID, Turner AK, Wilson JP, Jenson SK, Band LE (1993) GIS and land-surface-subsurface process modeling. In: Goodchild MFR, Parks BO, Steyaert LT (eds) Environmental modeling with GIS. Oxford University Press, New York, pp 196–230

Mulligan J, Wainwright M (2004) Modeling and model building. In: Mulligan J, Wainwright M (eds) Environmental modelling: finding simplicity in complexity. Jonh Wiley and Sons, Chichester, pp 7–74

Nearing MA, Pruski FF, O'Neal MR (2004) Expected climate change impacts on soil erosion rates: A review. J. Soil Water Conservation 59:43–50

Regione Campania (1998) Cartografia tecnica regionale. http://www.sito.regione.campania.it/territorio/regionecampania.htm. Accessed 24 Sept 2009

Renard KG, Foster GR, Weesies GA, McCool DK, Yoder DC (1997) Predicting soil erosion by water: a guide to conservation planning with the revised Universal Soil Loss Equation (RUSLE). USDA, Agricultural Handbook 703

Rovito PL (2001) From the 'amusing woods' to the 'sterile and slid' plains. Notes about the environment disaster in Campania. Rivista Storica del Sannio 16:297–338 (in Italian)

Salski A (2006) Ecological applications of fuzzy logic. In: Recknagel F (ed) Ecological informatics. Springer, Berlin, pp 3–14

Thornes JB (1990) The interaction of erosional and vegetational dynamics in land degradation: spatial outcomes. In: Thornes JB (ed) Vegetation and erosion. Jonh Wiley and Sons, Chichester, pp 45–55

Torri D, Poesen J, Borselli L (1997) Predictability and uncertainty of the soil erodibility factor using a global dataset. Catena 31:1–22

Toy TJ, Foster GR, Renard KG (2002) Soil erosion; prediction, measurement, and control. John Wiley and Sons, New York

Van der Knijff JM, Jones RJA, Montanarella L (2000) Soil erosion risk assessment in Italy, European Soil Bureau, JRC—Report EUR 19022EN

Vandewiele GL, Xu CY, Lar-Win N (1992) Methodology and comparative study of monthly water balance models in Belgium, China and Burma. J Hydrol 134:315–347

Wang G, Gertner G, Singh V, Shinkareva S, Parysow P, Anderson A (2002) Spatial and temporal prediction and uncertainty of soil loss using the revised universal soil loss equation: a case study of the rainfall-runoff erosivity R factor. Ecol Model 153:143–155

Wessolek G, Duijnisveld WHM, Trinks S (2008) Hydro-pedotransfer functions (HPTFs) for predicting annual percolation rate on a regional scale. J Hydrol 356:17–27

Wischmeier WH, Smith DD (1958) Rainfall energy and its relationship to soil loss. Trans Am Geophys Union 39:285–291

Wischmeier WH, Smith DD (1978) Predicting rainfall erosion losses: a guide to conservation planning. USDA, Agriculture Handbook No. 537. Government Printing Office, Washington

Zhang XC, Nearing MA (2005) Impact of climate change on soil erosion, runoff, and wheat productivity in central Oklahoma. Catena 61:185–195